Electrical Power and Energy Systems 147 (2023) 108876

Contents lists available at ScienceDirect

International Journal of Electrical Power and Energy Systems

journal homepage: www.elsevier.com/locate/ijepes

State relevance and modal analysis in electrical microgrids with high penetration of electronic generation ☆

Andrés Tomás-Martín [a,*], Aurelio García-Cerrada [a], Lukas Sigrist [a], Sauro Yagüe [b], Jorge Suárez-Porras [a]

[a] Institute for Research in Technology, ICAI, Comillas Pontifical University, Alberto Aguilera, 25, 28015, Madrid, Spain
[b] IQS Department of Industrial Engineering, Ramón Llull University, Barcelona, Spain

ARTICLE INFO

Keywords:
Distributed control
Dynamics
Reduced order systems
Modal analysis
State-relevance coefficient

ABSTRACT

A clean electricity sector requires distributed generation through electronic power sources with very fast voltage, frequency, and current responses. Therefore, unlike in conventional power systems with slow generators, fast power-line dynamics may not always be negligible compared to generators' dynamics. In this scenario, this paper proposes an algorithm to calculate the relevance of each state of a linear system in the system input–output response systematically. It explores its application to a linearised model of an electrical microgrid to decide which dynamics are relevant to be included for analysis and/or simulation. This algorithm uses a non-physical balanced realisation of the linear system, where the energy of each state variable in the system output can be calculated. Both the balanced realisation and the original system have the same eigenvalues. A "relevance coefficient" (RC) of each one of the state variables of the original linear system has been defined by combining the relevance of the states of the balanced system with the mode-in-state participation factors of the system eigenvalues of both systems. The usefulness of the proposed RC was validated by comparing detailed nonlinear simulations of an electrical microgrid with nonlinear simulations of reduced models as informed by the RC. Results show that the proposed RC gives sensible and clear recommendations even in systems without a clear time separation between system dynamics.

1. Introduction

Microgrids are considered fundamental tools for the penetration of renewable energy resources (RERs) by means of distributed generation (DG). Since RERs nearly always require the contribution of power electronics, microgrids are bound to be populated by electronic converters, which make tight and fast control possible. Among those converters, DC-to-AC voltage-source converters (VSCs) are nowadays considered the most flexible and viable alternative to interface RERs to the AC system. A microgrid can operate in a stand-alone manner (often called "islanded") or tight to a larger and stronger electric grid. For the purpose of this paper, the former case is the one of interest.

The analysis and simulation of conventional power systems have relied on a clear time-scale separation between slowly-varying electromechanical variables, such as voltage and speed of synchronous generators, and fast-varying electromagnetic variables, such as line currents and bus voltages. This has led to the use of algebraic equations to describe the latter, and differential equations to describe the former when studying stability problems (most noticeably, small-signal and transient frequency and angle stability) [1]. Since the order of a dynamic system is measured by the number of differential equations used to describe it, this separation provides a model-order reduction naturally [2]; however, the growing use of fast VSC-based generation raises doubts about whether the model reduction based on time-scale separation solely is still applicable. Ref. [3] simplifies level-0 of converter control by considering either the current control or the current+voltage control instantaneous. Ref. [4] proposes the use of hybrid network models for small-signal stability analysis of power systems with fast-acting VSC-based stations of high-voltage direct-current (HVDC) and flexible alternating current transmission systems (FACTSs): algebraic equations are used to describe lines far away from a VSC, whereas detailed differential equations are used to describe lines close to VSCs. Results in [4] show that this hybrid approach produces more accurate

☆ This work has been partially financed through the research program S2018/EMT-4366 PROMINT-CAM on Smart Grids of Madrid Government, Spain, with 50% support from the European Social Fund and by Grants RTI2018-098865-B-C31 and RTC-2017-6296-3 funded by MCIN/AEI/10.13039/501100011033 and by "ERDF A way of making Europe".

* Corresponding author.
E-mail address: atomas@comillas.edu (A. Tomás-Martín).

https://doi.org/10.1016/j.ijepes.2022.108876
Received 20 July 2022; Received in revised form 14 November 2022; Accepted 29 November 2022

modal results than the traditional one and prevents the computational complexity that would arise if all power lines were modelled in detail. More recently, [5] assessed the impact that a simplified model of the AC network has on the accuracy of small-signal stability analysis of AC systems with VSC-based HVDC. Ref. [5] revisits the use of hybrid models such as the ones proposed in [4] and reveals the importance of detailed models of AC-line and phase locked loops (PLLs) in critical situations with low short circuit ratio (SCR) or very long lines in the vicinity of VSCs. Finally, a very recent work [6] goes further and shows that complex AC-line models are necessary to study the dynamics of power systems with VSCs if high-frequency phenomena such as harmonic stability [7] or electromagnetic converter interactions [8] are to be addressed reliably. This reference proposes an algorithm to determine how far we can go simplifying complex AC-line models, as proposed in [9], while satisfying a given accuracy threshold. The simplification of AC-line models has probably been the topic given the most attention in the literature. Still, the always-increasing complexity of the application and control of VSCs calls for a more comprehensive analysis of whether the dynamics of some parts of modern power systems can be neglected for simulation, analysis or control purposes, leading to reduced-order models.

In the scenario described above, this paper presents a systematic algorithm to extract the relevant physical states of a dynamic system in its input–output response, and applies it to microgrids with electronic power sources. Once the relevant states are identified, one can proceed to apply any model-reduction technique to include the dynamics of those variables in a reduced-order model of the microgrid. This model can then be used for nonlinear simulation or modal analysis, for example. In general, the selection of relevant states is usually made in terms of the associated time constants only, neglecting other state characteristics. The proposed algorithm combines the energy-in-state information provided by a balanced linear approximation of the nonlinear system of the microgrid and the mode-in-state participation factors of a linear approximation of that nonlinear system to determine the RC. Notice that the dynamics of nonlinear systems are often studied by using the eigenvalues (or modes) of a linear approximation of that system.

Given a nonlinear state variable description of a dynamic system, a balanced linear approximation (or realisation) of the model is often used to assess which states participate with more energy in the output response of the system. This information is obtained by using the so-called Hankel singular values (HSVs) and can be used to decide, by eliminating low-energy states (truncation), which state variables one should include in the next step, namely, the order reduction of the model [10]. Unfortunately, the state variables of the balanced realisation are not those of the original system but are obtained by using a linear transformation from the latter. Nevertheless, this method has been used for model order reduction (MOR) in power systems [11], resulting in a much lower order reduced system. If the error between the response of the original system and the reduced-order one is to be minimised, the Hankel-norm (sum of the HSVs of the neglected states) must be minimised [12].

MOR techniques applied to dynamic systems include the so-called "moment-matching techniques" (also known as Krylov-based techniques), which are transfer-function-based methods whose objective is to match the behaviour of the first terms of the power series expansions of the system. A moment-matching method commonly used to approximate communication delays is Padé's approximation [13]. These techniques are widely used to have a reduced-order model that precisely describes the frequency response of the original model; however, the relation between the original states and the system dynamics is unclear.

Singular perturbation techniques are also popular MOR algorithms [14]. They have been applied to microgrids in [15], where the authors cluster a group of eigenvalues with slow time constants and select the relevant states as the most participated by each of those eigenvalues. This reference also includes an approach that computes a reduced-order model (not a simple truncation) with eigenvalues that are close to the selected ones in the original model; however, only the time constants of the system eigenvalues are considered to select which variables must be included in the reduced-order model. Neither eigenvalue damping nor its weight in the system response is taken into account, and this shortcoming can be tackled by using the RC proposed in the present paper. A similar MOR algorithm using singular perturbation can be found in [16]. Ref. [2] compares balanced truncation and Krylov-based techniques to reduce the model order in power systems. The so-called balanced residualisation calculates the balanced realisation of the model and then reduces the model using singular perturbation [17].

Ref. [18] uses a state-space transformation that clarifies the eigenvalue-state dependence; however, it also focuses only on the time constants of the eigenvalues to consider them in the subsequent model reduction. In fact, approaches that keep the system structure and the physical meaning of the states in reduced models, either make assumptions valid for conventional power systems but not necessarily for electronics-dominated power systems, or they focus on selecting the eigenvalues with the slowest time constants and the states participated by those eigenvalues (modal analysis). The present paper systematises the selection of relevant states by evaluating the RC.

This paper is organised as follows: Section 2 explains the proposed algorithm. Section 2.1 introduces the concept of balanced realisation of a linear system. Sections 2.2 and 2.3 spell out the algorithms to calculate the eigenvalue and the state RCs, respectively. The algorithm will then be applied to two microgrids of different sizes with a hierarchical control system to identify the relevant states and reduce the model order. These microgrids are powered by grid-forming VSCs (*i.e.*, electronic power converters imposing voltage and frequency to the point of coupling, also known as VCVSCs). Section 3 explains how the example microgrids are modelled and controlled. Section 4 presents the results obtained when applying the proposed state RC to a small microgrid and the impact of varying system and control parameters on RCs is explored. A larger microgrid is studied in Section 5. Section 6 provides some further and related applications of RCs. Finally, Section 7 concludes the paper.

2. The state relevance calculation algorithm

MOR in any linear system involves:

1. Identification of relevant dynamics
2. Identification of the states participated by those relevant dynamics
3. Reduction of the model to include the dynamics of the relevant states plus the algebraic equations to calculate the non-relevant states

The proposed algorithm focuses on the two first items of the list above, namely, the identification of relevant dynamics and states of the system. To calculate the state-relevance coefficient, the algorithm includes three steps: (a) calculation of a balanced realisation of the linear system; (b) calculation of the relevance of its eigenvalues; and (c) calculation of the relevance of the states of the original system.

2.1. Balanced state-space realisation of a linear system

Let us consider a typical description of a linear system of the form:

$$\begin{cases} \dot{x} = \mathbf{A}x + \mathbf{B}u \\ y = \mathbf{C}x + \mathbf{D}u \end{cases} \tag{1}$$

where x is the system state column vector, u is the input vector, y is the output vector, and $\mathbf{A}$, $\mathbf{B}$, $\mathbf{C}$ and $\mathbf{D}$ are the system matrices.

If the system in (1) is asymptotically stable, the controllability ($\mathbf{W}_c^2$) and observability ($\mathbf{W}_o^2$) Gramians are defined as [19] (superscript T means the transposed of a matrix or vector):

$$\begin{cases} \mathbf{W}_c^2 \triangleq \int_0^\infty e^{\mathbf{A}t}\mathbf{B}\mathbf{B}^{\mathrm{T}}e^{\mathbf{A}^{\mathrm{T}}t}\,\mathrm{d}t \\ \mathbf{W}_o^2 \triangleq \int_0^\infty e^{\mathbf{A}^{\mathrm{T}}t}\mathbf{C}^{\mathrm{T}}\mathbf{C}e^{\mathbf{A}t}\,\mathrm{d}t \end{cases} \tag{2}$$

The linear system in (1) can be transformed into another one whose states $\overline{x}$ are a linear combination of the states of the original system (x) given by a transformation matrix $\mathbf{T}$ such that $\overline{x} = \mathbf{T}x$ and $x = \mathbf{T}^{-1}\overline{x}$ [10]. The original linear system is consequently transformed into:

$$\begin{cases} \dot{\overline{x}} = \mathbf{T}\mathbf{A}\mathbf{T}^{-1}\overline{x} + \mathbf{T}\mathbf{B}u \\ y = \mathbf{C}\mathbf{T}^{-1}\overline{x} + \mathbf{D}u \end{cases} \tag{3}$$

and the new controllability and observability Gramians are:

$$\overline{\mathbf{W}}_c^2 = \mathbf{T}\mathbf{W}_c^2\mathbf{T}^T \qquad \overline{\mathbf{W}}_o^2 = (\mathbf{T}^{-1})^T\mathbf{W}_o^2\mathbf{T}^{-1} \tag{4}$$

A balanced realisation in (3) means that:

$$\overline{\mathbf{W}}_c^2 = \overline{\mathbf{W}}_o^2 = diag(g_i) \tag{5}$$

where g_i are the HSVs. Small entries in g_i indicate states that can be removed to simplify the model since both their observability and controllability are small, whereas large entries indicate the most relevant states [19]. Since the states of the balanced system are a combination of the states of the original system, the former states may not have physical meaning anymore.

2.2. Eigenvalue-relevance analysis

Since the balanced transformation is linear, the transformed system has the same eigenvalues as the original system; therefore, relevant eigenvalues of the transformed system will also be relevant eigenvalues of the original system. Relevant states of the transformed system can be chosen based on the values of g_i after the transformation in (3)–(5), and relevant eigenvalues can be determined by checking which eigenvalues have high participation factors in the relevant states. The mode-in-state participation factors normalised as in [20] (based on [21]) are used here:

$$p_{ji} = \frac{\left|w_{ij}\right|\left|v_{ji}\right|}{\sum_{\forall k}\left|w_{ik}\right|\left|v_{ki}\right|} \tag{6}$$

where p_{ji} is the normalised mode(i)-in-state(j) participation factor in a linear system, v_{ji} is the element of the jth row and ith column of matrix $\mathbf{V}$ of right column eigenvectors and w_{ij} is the element of the ith row and jth column of matrix $\mathbf{W}$ of left row eigenvectors calculated as $\mathbf{W} = \mathbf{V}^{-1}$. Notice that whereas v_{ji} and w_{ij} are complex numbers, in general, p_{ij} is always a real number greater than 0. A decentralised calculation of eigenvalues and eigenvectors is out of the scope of this paper. Some results can be found in the literature [22].

Since each state of the transformed system has a different relevance, it is proposed that the participation factor of each eigenvalue in the states of the transformed system should be weighted with the state relevance (*i.e.*, an eigenvalue having a high participation factor in a relevant state is not necessarily more relevant than an eigenvalue having a low participation factor in a more relevant state). The value of g_j can then be used to weight $\bar{p}_{ij}$ using:

$$\hat{\mathbf{R}}_\lambda = [\hat{R}_\lambda(\lambda_1), \ldots, \hat{R}_\lambda(\lambda_n)]^T = \left([g_1, \ldots, g_n] \cdot \overline{\mathbf{P}}\right)^T \tag{7}$$

where $\hat{R}(\lambda_i)$ will be called the "relevance of eigenvalue λ_i" and $\overline{\mathbf{P}}$ is the participation matrix of the transformed system which has $\bar{p}_{ij}$ in its ith row and jth column. The bar above $\mathbf{P}$ and its elements has been used to indicate that they have been calculated using the balanced realisation in (3). Normalising yields:

$$\mathbf{R}_\lambda = \left[R_\lambda(\lambda_1), \ldots, R_\lambda(\lambda_n)\right]^T = \hat{\mathbf{R}}_\lambda / max(\hat{\mathbf{R}}_\lambda) \tag{8}$$

The normalised value will be used unless otherwise stated.

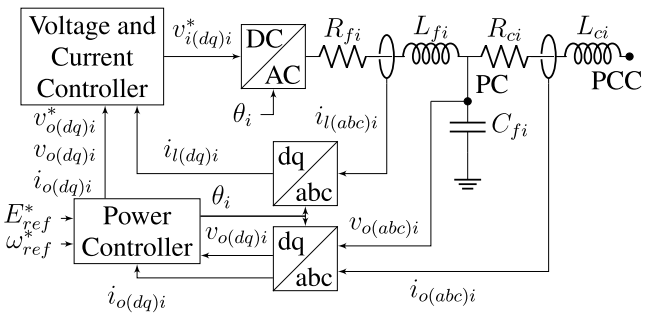

Fig. 1. Schematics of a VCVSC. The abc/dq block is the so-called Park Transform. *Source:* Adapted from [23].

2.3. State relevance

Let us now weigh each column of the participation matrix of the original system ($\mathbf{P}$) with the relevance of its associated eigenvalue ($\hat{R}(\lambda_i)$). By summing all these weighted columns, the resulting column vector can be used to quantify the "relevance of each state":

$$\hat{\mathbf{R}}_x = \mathbf{P} \cdot \mathbf{R}_\lambda \tag{9}$$

which can be normalised as follows:

$$\mathbf{R}_x = \left[R_x(x_1), \ldots, R_x(x_n)\right]^T = \hat{\mathbf{R}}_x / max\left(\hat{\mathbf{R}}_x\right) \tag{10}$$

where $R_x(x_i)$ will be called the "relevance coefficient (RC) of state x_i". The normalised value will be used unless otherwise stated.

3. Modelling and control of microgrids

The proposed RC will be applied to microgrids consisting of several DGs based on VCVSCs. The control of microgrids is typically a hierarchical control and the dynamic response of the microgrid is affected by level-0, primary, and secondary controls. These three levels will be modelled explicitly here.

The schematic of each VCVSC is shown in Fig. 1. It is connected to a bus or point of common coupling (PCC) and imposes the voltage and frequency on its point of control (PC). For several important reasons, this type of electronic converter is usually equipped with inner current and voltage controllers. Typically, PI voltage and current controllers in a synchronously rotating reference frame ($d-q$) guarantee that voltage and current follow their set points [23].

The abc/dq block in Fig. 1 is the so-called Park's Transform, which converts the balanced 3-phase voltage (or current) signal to its direct-quadrature (d – q) "components" in a reference frame that rotates with the frequency of the 3-phase signal imposed by the VCVSC. In this reference frame, d – q components of all electrical variables are constants in steady-state in balanced 3-phase systems, and simple PI controllers for power control, voltage control, or current control are effective. Each VCVSC uses its reference frame for the Park's transform for control purposes such that the set-point for its q component is zero ($v^*_{oqi} = 0$). Applying a power-invariant Park's Transform, active and reactive power drawn from a VCVSC have a similar expression to the one using three-phase (abc) electrical variables. For modelling and simulation purposes of the whole system, one of the $d-q$ synchronous reference systems is taken as the angle reference, and all other state variables are referred to it.

The simplest model of a VCVSC is an ideal voltage source that imposes the voltage and frequency at its PC. Including the voltage and current controllers makes the model more accurate, which is, in general, necessary for stability studies related to converter interactions. Typically, the converter itself (*i.e.*, the DC/AC conversion block in Fig. 1) is modelled as a controlled ideal sinusoidal voltage source by

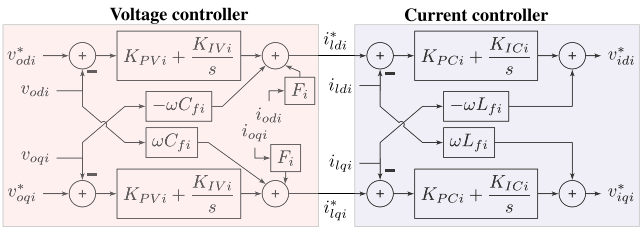

Fig. 2. Voltage and current controllers of a VCVSC (i), including the decoupling of the output LC filter and current feed-forward.
Source: Adapted from [24].

neglecting the PWM-driven switching of the switches (*e.g.*, IGBTs) because switching transients are much faster than the dynamics of voltage and current controllers. Given the rather fast controller dynamics, line dynamics of the microgrid cannot be neglected a priori. Obviously, the presence of several VCVSCs and other elements, together with the inclusion of line dynamics, significantly increases the size of the problem with respect to traditional power systems where power-line and generator-stator dynamics are most often neglected.

A typical control level-0 (*i.e.*, output current and voltage controllers) of a VCVSC [24] is shown in Fig. 2.

If more than one VCVSC must work in parallel, some form of power sharing should be applied, for example by means of a droop control. Fig. 3 illustrates the $\omega-P$ and $v-Q$ droop controllers of a VCVSC used in this case study, where the actual active and reactive powers delivered by each converter i (P_i and Q_i, respectively) are calculated from its output voltage and current. The filtered results are used to manipulate the output voltage and frequency set-point values.

A secondary control layer has also been implemented in the system shown in Fig. 6. It takes the form of a multi-agent-based distributed secondary control which will be later extended to a larger system in the paper. Unlike in a centralised controller, the generators must collaborate to reach a solution, called "consensus value". Multi-agent-based control is attractive for microgrids, given the dispersed nature of RERs. Ref. [25] includes more details on cooperative multi-agent secondary control applied to microgrids, along with the conditions that the communication graph must meet to have a stable system.

Figs. 4 and 5 show the multi-agent secondary control of each VCVSC used in this paper. In general, VCVSC$_i$ receives information from its neighbours (j) if $a_{ij} \neq 0$ and T_d represents a constant communication time delay from DGj to DGi. Only one VCVSC (the leader) knows the frequency and voltage reference values (ω_{ref} and v_{ref}, respectively) and has $g_i = 1$.

The secondary control structure in Figs. 4 and 5 is based on the one included in [23] for a VCVSC. In this application, VCVSCs will not seek voltage consensus ($B = 1;\ \beta = 0$) to make consensus in reactive-power sharing possible. In systems with highly inductive transmission lines, the reactive-power transfer between two points mostly depends on the voltage difference; therefore, voltage profile and reactive power flow cannot be controlled simultaneously (as explained in [26]). A very small, constant communication delay between the two converters was included to show that the state relevance finds it negligible. A thorough analysis of the effect of communication delays is out of the scope of this paper. Delays are modelled using a third-order Padé approximation in the linear model and an exact delay in the nonlinear model.

The complete model for each VCVSC has 14 states (see Fig. 1 for the explanation of all variables), corresponding to the inner and outer inductor currents ($i_{l(dq)}$ and $i_{o(dq)}$), the capacitor voltage ($v_{o(dq)}$), the filters for active and reactive power (P_f and Q_f), integrators of the frequency (ω^*) and voltage (E^*) secondary controllers, integrators of the voltage and current controllers ($PIv_{(dq)}$ and $PIi_{(dq)}$). The complete model can be found in Appendix B. The leader DG has been chosen as the angle reference, which will be assigned here without loss of generality to DG1, and therefore, for any other converter, $\theta_i = \int(\omega_i - \omega_{DG1})$.

Table 1
Parameters used for the simulation of the microgrid.

VCVSCs			
m_P	$9.42 \cdot 10^{-4}$ rad/sW	n_Q	$1.14 \cdot 10^{-3}$ V/VAr
R_f	0.4332 Ω	L_f	13.7892 mH
C_f	73.4787 μF	R_{cf}	4332 Ω
R_c	0.4332 Ω	L_c	13.7892 mH
K_{PV}	0.023084	K_{IV}	0.23084
K_{PC}	43.32	K_{IC}	433.2
F_i	1	LPF_{const}	0.01 s
Sec. control parameters and bases			
c_f	100	c_v	100
f_{base}	50 Hz	S_{base}	10 kVA
delay (T_d)	$1.00 \cdot 10^{-3}$ s	$V_{nom} = V_{base}$	380 V
Z_{base}	43.32 Ω	$\beta = 0$	$B = 1$
$g_1 = 1$	$g_i = 0\ \forall\ i \neq 1$	$a_{ij} = 1\ \forall\ i \neq 1,\ j = i - 1$	
Lines			
R_{line}	0.4332 Ω	L_{line}	13.7892 mH
Load 1			
R_{load}	21.66 Ω	L_{load}	68.9459 mH
Other loads			
R_{load}	43.32 Ω	L_{load}	137.8918 mH

4. Case study 1: Small microgrid

4.1. Description of the case study

The RC described above is used to investigate a small microgrid consisting of two VCVSCs (DG1 and DG2) connected to two buses, a load connected to each bus (Load 1 and Load 2) and a power line connecting the two buses (see Fig. 6).

The current case study results in a very simple graph in which DG1 has been made leader and angle reference, with set points $v_{ref} = 1$ pu and $\omega_{ref} = 1$ pu, and in which DG2 follows the frequency and active and reactive power sharing of DG1. Table 1 shows control level-0 parameters, droop-controller parameters, distributed secondary control parameters, and system parameters. Note that the primary and level-0 controls do not exhibit a very clear time-scale separation on purpose. The parameters of the test system are based on those in [24].

This simple case study will be used to illustrate the use of RC. Firstly, the impact of varying parameters on the RC is shown. Secondly, the RC is used to support the MOR of the small microgrid. Nonlinear simulations are used to compare the proposed approach with other approaches to select relevant states. Finally, the impact of the time-scale separation of the controls on the RC is analysed.

4.2. Illustration of the RC

The system in Fig. 6 has been linearised around the operating point shown in Appendix A by using MATLAB® and Simulink® for different cases to illustrate the use of the state RC. Line, loads, and controller dynamics have all been included. To linearise the system, the references for the frequency and voltage of the leader and the load disturbance have been set as inputs. Frequency, voltage, and active and reactive power of all converters have been set as outputs. Notice that the calculation of the balanced realisation of the linear model depends on the input–output choice.

The value of the RC has been calculated for all the state variables of the model in Fig. 6, once linearised, by following the procedure described in Sections 2.1–2.3 and the relevance of some states has been investigated in various circumstances. For example, Fig. 7a shows the value of the RC for the most relevant of the delay-related states as the delay transmitting the value of ω from DG1 to DG2 changes from 0.001 to 0.1 s while maintaining the delay transmitting the values of P and Q equal to 0.001 s. Clearly, the larger the delay is, the more relevant

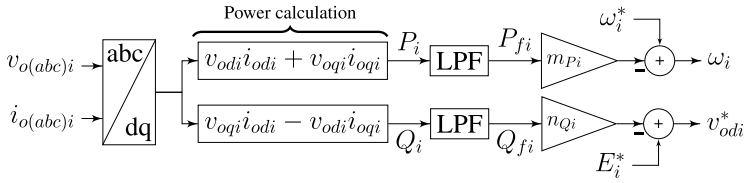

Fig. 3. Power controller of a VCVSC (i), including droop control for frequency and voltage. low-pass filters (LPFs) are included to reduce measurement noise.

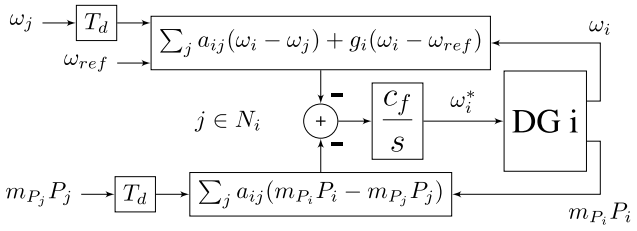

Fig. 4. Multi-agent secondary ω-P control of a VCVSC (i) with N_i neighbours.

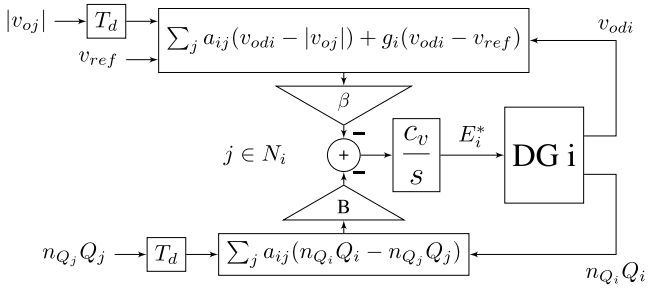

Fig. 5. Multi-agent secondary v-Q control of a VCVSC (i) with N_i neighbours.

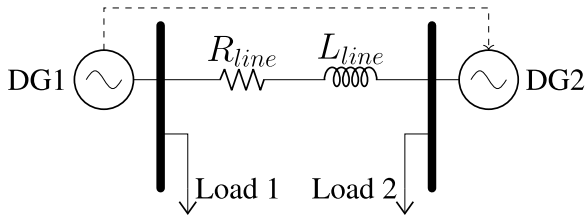

Fig. 6. A case study with two VCVSCs and two loads. A dashed line represents a communication link between the two VCVSC.

its related state is, whereas the relevance of constant delays does not change much. In fact, when the delay transmitting ω is increased to around 0.04 s, its states are the most important ones in the input–output response of the system (highest RC).

Similarly, Fig. 7b (blue line) shows the value of the relevance coefficient for the most relevant of the power-line-related states as the X/R ratio changes from 0.2 to 20 while maintaining the line impedance modulus equal to 0.1005 pu.

Clearly, the transmission-line dynamics can be neglected if its X/R ratio is low; however, it must be considered if the X/R ratio increases (the line time constant also increases).

4.3. Applying the state RC to MOR

This section investigates whether the state RC is helpful in the reduction of the linear model of a microgrid. Three approaches have been used:

1. The state RC has been used to decide which states should be eliminated from the model. This approach will be called "Rel.".

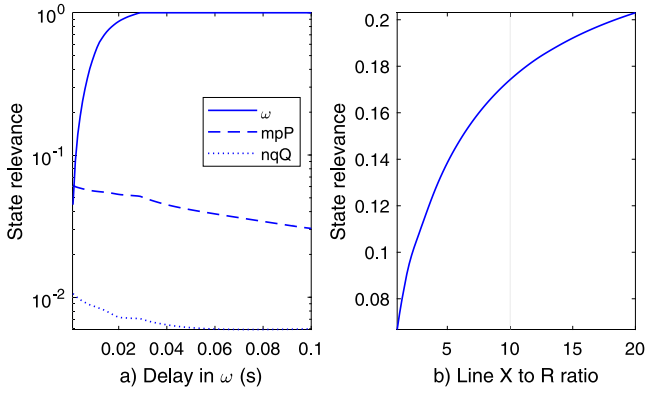

Fig. 7. (a) Relevance of the most relevant delay-related states in the transmission of ω (continuous line), mpP (dashed line), and nqQ (dotted line), separately. (b) Relevance of the transmission-line-related state when changing its X/R ratio. The vertical line represents the original value of the X/R.

2. The states participated by eigenvalues with small time constants (fast dynamics) have been eliminated. This approach will be called "Eig.". It is used by conventional MOR techniques, including [15].
3. Since fast dynamics are often neglected in MORs, strategy "Rel." has been simplified by assessing eigenvalue relevance as $\hat{\mathbf{R}}_\lambda = -1/\mathrm{Real}(\lambda_i)$ instead of using (7). The eigenvalue relevance is then used to calculate the state relevance using (9) and (10). The state-relevance coefficients $\mathbf{R}_x$ calculated this way have been used to decide which states can be eliminated. This approach will be called "Rel. ap.".

Fig. 8 illustrates how the system eigenvalues participate in the states of the original system. Mode-in-state participation factors have been calculated by using (6). Notice that a dark grey colour indicates those states with a large participation of a given mode. Each tic in the X-axis represents an eigenvalue. They have been sorted in ascending order according to their time constants ($-1/\mathrm{Real}(\lambda_i)$) which have been explicitly recorded at the bottom of the figure to show which states are participated by the fast or slow eigenvalues. States have been grouped on the Y-axis (for example, delay states and d-q axes in currents and voltages).

Fig. 8 shows that eigenvalues 1 to 4 have an exponential time constant just above 10^{-6} s. Furthermore, states of the time-delay blocks ($Delay\,\omega$, $Delay\,m_pP$, $Delay\,n_qQ$) are participated by the eigenvalues with small time constants. Notice that $Delay\,n_qQ$ has no participation factors for being smaller than 0.01. Voltage- and current-controller states (named $DG1-2PIi$ or $DG1-2PIv$) are participated by the eigenvalues with the largest time constants. Transmission line, low-pass power filters, and secondary-control states are participated by eigenvalues with time constants from just above 10^{-5} s to just below 10^{-1} s. Intentionally, time scales between primary and level-0 controls have not been separated.

Fig. 9 shows the accumulated relevance of the states of the original system by following the procedure described in Sections 2.1–2.3. The accumulated relevance of the states can help to decide how many states

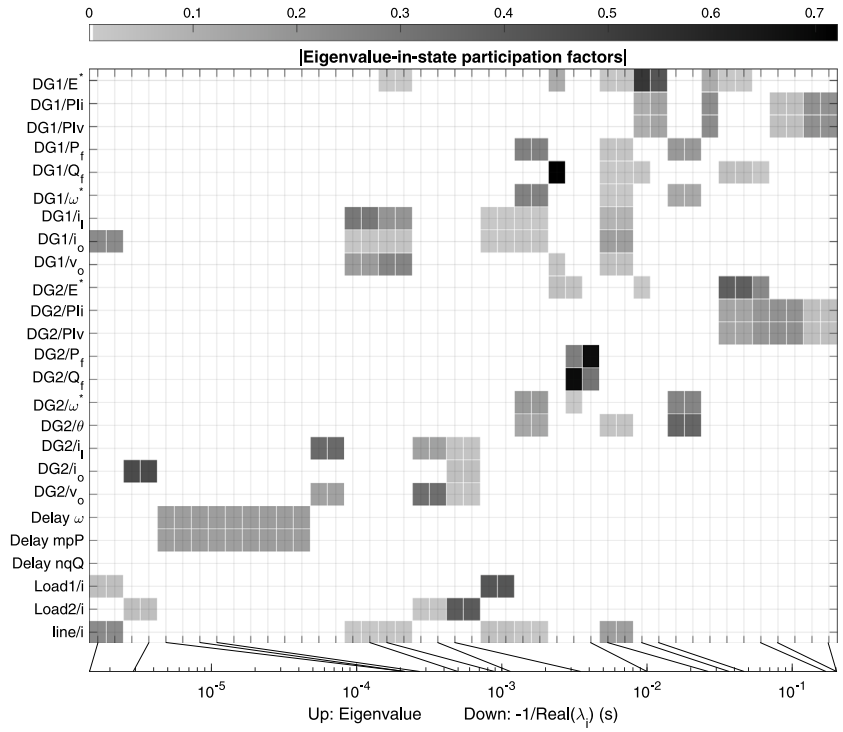

Fig. 8. Illustrating the participation factors of the eigenvalues in the states of the system. For clarity, participation factors below 0.01 are not shown.

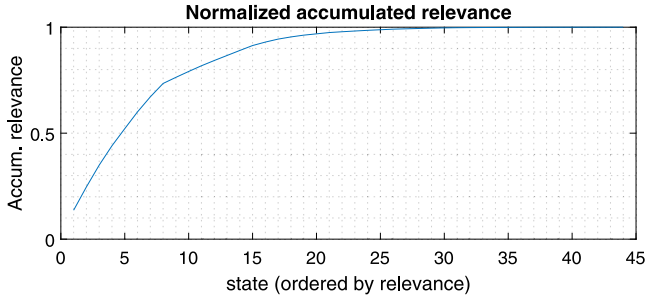

Fig. 9. Accumulated relevance of the states of the original system. Case study 1 with no clear time-scale separation.

to include in the reduced system. After state number 8, there is a visible change in the slope of the curve and taking 14 states one reaches 90% of the final value of the accumulated relevance.

Table 2 shows and compares the three different approaches to select relevant states. Columns $R_{x,1}$ and $R_{x,2}$ in Table 2 show the state relevance calculated in approaches "Rel." and "Rel. ap.", respectively. Motivated by the slope change in Fig. 9, eight states will be chosen to be included in a reduced-order model. From columns $R_{x,1}$ and $R_{x,2}$, the eight most relevant states have been chosen and highlighted in Table 2. The eight states chosen by looking only at the largest time constants of the linear system eigenvalues and the mode-in-state participation of those eigenvalues have been highlighted in column x_3 in Table 2.

Table 2 shows that the three reduced systems include the following states:

- "Rel." includes the reference frame of DG2, the secondary control of both converters, the low-pass filter (LPF) of the active power of DG1, the output inductance of DG1, and the voltage and current controller of DG2.
- "Rel. ap." and "Eig." include the voltage secondary control of DG2 and the voltage and current controllers of both converters.

Clearly, several states that the proposed method finds negligible in the system response are included in the other two approaches. The question arises whether the RC-informed selection outperforms the other two approaches. The accuracy of the reduced models suggested by the three approaches presented will be investigated by means of simulations of the reduced nonlinear models. The procedure followed to reduce the nonlinear models, according to the relevant states as identified by the three approaches, is described in Appendix C (*e.g.*, in variables with fast dynamics, their derivatives are made equal to zero and in control systems, output variables follow their references instantaneously).

Fig. 10 shows the response of several electrical variables of DG2 in the original (complete) and reduced nonlinear models to a change in Load 1. The load change is simulated by reducing the impedance of Load 1 a 50% suddenly while keeping its X/R ratio; therefore, the active and reactive powers consumed by Load 1 increase. The reduced models used for the simulation in that figure include the states highlighted in Table 2 plus some additional ones because the reduction was done respecting natural blocks (*e.g.*, if the d axis of the voltage and current controller of a converter are suggested to be included in the reduced model, the q axis must also be included). Moreover, the filter dynamics are also included due to the structure of the model. The total number of states used in the simulation of each of the reduced-order models has been noted, enclosed within brackets, in Fig. 10.

Clearly, the proposed method "Rel." can represent the original system dynamics more accurately with fewer states than the other two methods. Furthermore, the proposed method is the only one having a response of DG2 frequency similar to the original system response.

4.4. Impact of control time-scale separation

The microgrid shown in Fig. 6 was linearised with the parameters shown in Table 1, except for the following modifications in some VCVSC parameters:

$$m'_p = 10 \cdot m_p, \quad n'_q = 10 \cdot n_q, \quad c'_f = c'_v = 2,$$
$$T'_f = 1\,\text{s}, \quad \text{delay}' = 1 \cdot 10^{-5}\,\text{s}.$$

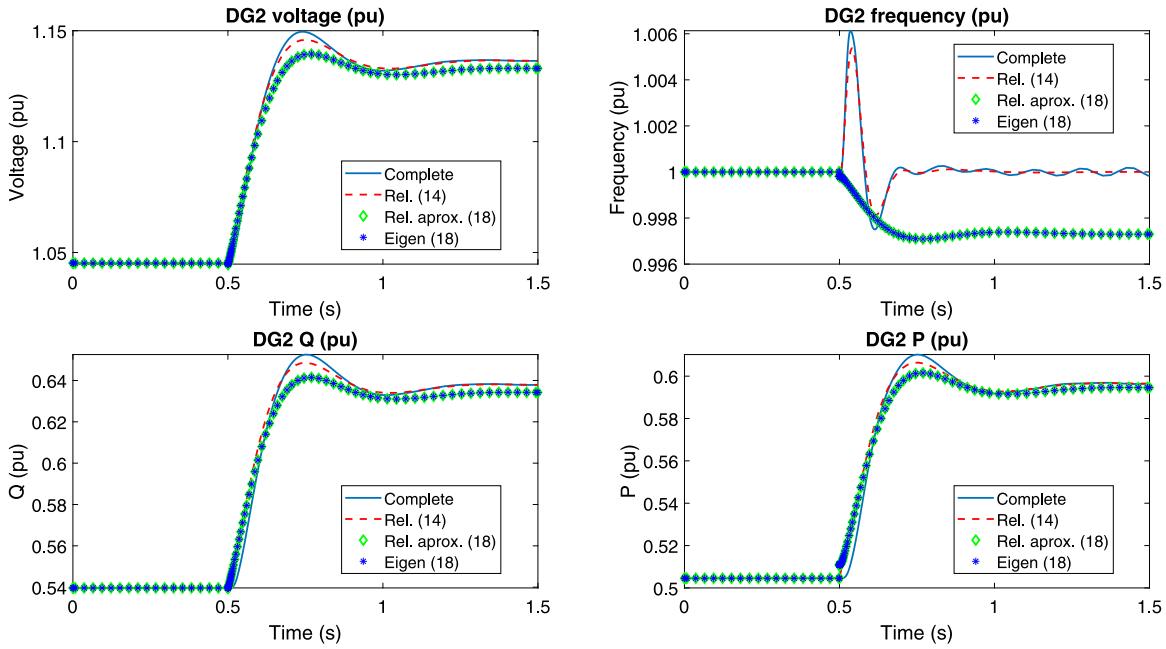

Fig. 10. Response of DG2 in case study 1 to a 50% reduction in the impedance of Load 1 (but constant X/R ratio). In legend, enclosed within brackets are the numbers of states included in the reduced models. Not a clear time-scale separation.

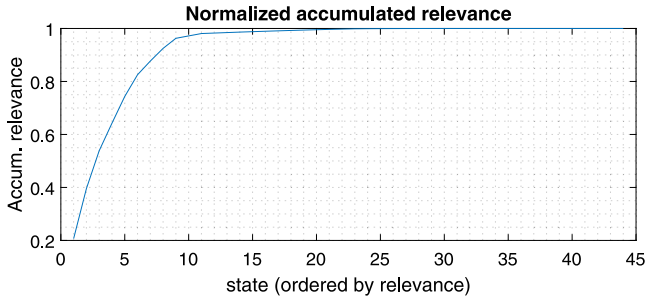

Fig. 11. Accumulated relevance of the states of the original system. Case study 1 with a clear time-scale separation.

These changes slow down the secondary control and the power filter dynamics and clarify the time-scale separation of the system dynamics.

Fig. 11 shows the accumulated relevance of the states of the original system. Clearly, the first nine states are the most relevant ones and the rest of the states do not contribute much.

Columns $R_{x,1}$ and $R_{x,2}$ in Table 3 include the state relevance for the test system calculated according to alternatives 1 and 3 in Section 4.3 and the nine states with the highest relevance have been highlighted to be selected in reduced models. Column x_3 of the same table shows that the dynamics with high participation factors of the nine slowest eigenvalues coincide with those selected by the other two algorithms, unlike in Table 2. The three approaches suggest the inclusion of the same nine states, namely, the secondary control, and the power filter dynamics of both converters. The state involved in the reference frame calculation for DG2 must also be included.

Fig. 12 shows the response of several electrical variables of DG2 in the original and reduced nonlinear models to a change in Load 1 (a 50% reduction of load impedance but constant X/R ratio). The three reduced models include the same states and produce the same results.

5. Case study 2: a larger microgrid

A microgrid test system including ten VCVSCs has been used to investigate the application of the proposed state relevance coefficient in a larger system, where MOR techniques may be more helpful. The diagram of the microgrid for this case study is shown in Fig. 13. It is a radial extension of the small microgrid built with several blocks like the one in Fig. 6.

With the communication graph shown in Fig. 13, the values of a_{ij} and g_i in Figs. 4 and 5 for this case study are: $a_{ij} = 1$ if $i \neq 1$ and $j = i - 1$, otherwise $a_{ij} = 0$, and $g_i = 1$ if $i = 1$, otherwise $g_i = 0$. For simplicity, the microgrid was designed as a radial microgrid with equal converters and with each converter connected to the same bus as its local load. Radial microgrids could arise in distribution networks in which distributed generation is connected to intermediate nodes [27].

The parameters of the VCVSCs converters, lines and loads are the same as those in case study 1 (Table 1). The operating point around which the nonlinear system is linearised is shown as the power flow solution in Table A.6, included in Appendix A.

Fig. 14 shows the accumulated relevance of the states of the original system. In this case, the choice of how many states must be included in the reduced system is not very clear. The optimal value is between 50 and 100 states. To test the accuracy of the proposed method against others, even considering fewer states, three nonlinear reduced-order models have been compared: (a) a model including the 57 states with the largest relevance coefficients according to strategy 1 in Section 4.3; (b) a model including the 90 states with the largest relevance coefficients according to strategy 3 in Section 4.3, and (c) a model including the 90 states participated by the eigenvalues with the largest time constants. Again, the final number of states needed in the reduced models may differ (it may be higher due to structural considerations).

Fig. 15 shows the response of several electrical variables of DG10 in the original and reduced nonlinear models to a change in Load 1. The load change is simulated by reducing the impedance of Load 1 a 50% while keeping its X/R ratio.

Since the proposed method is the only one that finds the secondary control of all converters relevant, it is the only one having correct steady-state values. Moreover, it is the one with the best accuracy in the input–output response.

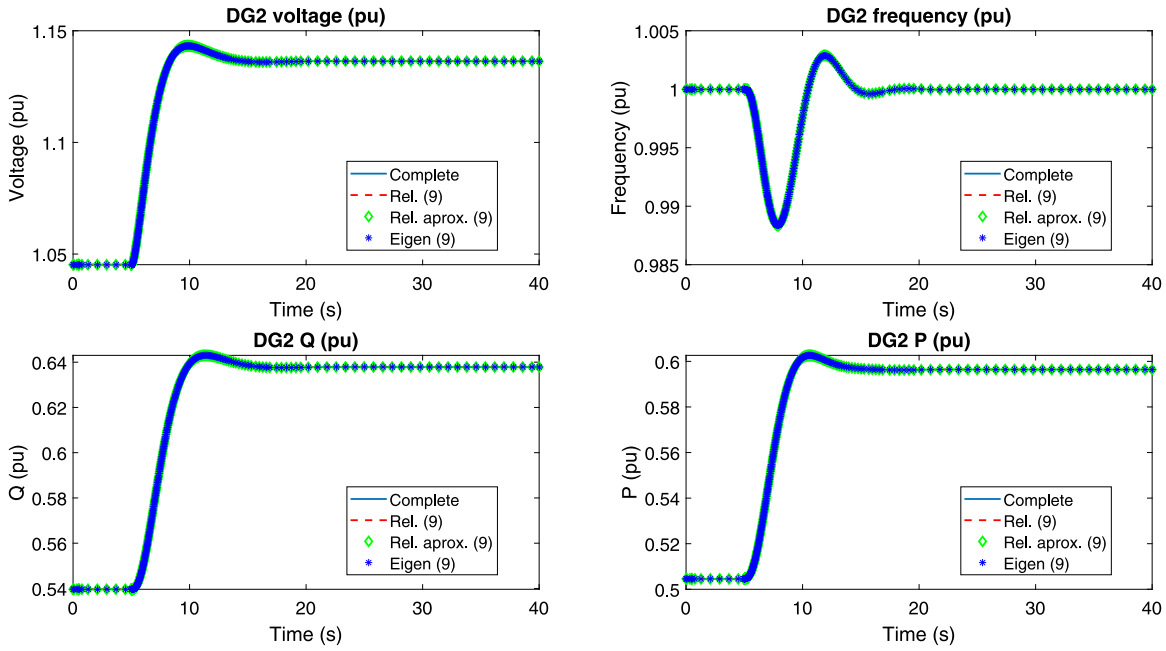

Fig. 12. Response of DG2 in case study 1 to a 50% reduction in the impedance of Load 1 but constant X/R ratio. Numbers enclosed within brackets in the legends show the number of states included in the reduced models. A clear time-scale separation.

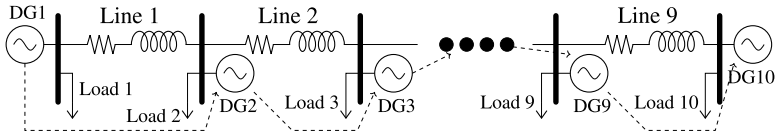

Fig. 13. Simplified diagram of the microgrid with ten VCVSCs (case study 2). A dashed line shows the communication graph, including the direction of the information.

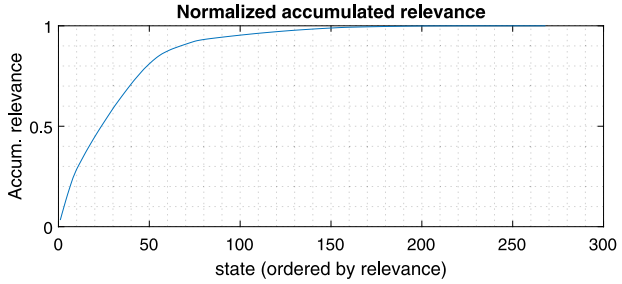

Fig. 14. Accumulated relevance of the states of the original system. Microgrid with ten VCVSCs (case study 2).

6. Further and related analysis of state RCs

6.1. Analysis of the importance of the communication graph

In addition to the identification of relevant states for MOR, the state RC can help to analyse the importance of each state in the input–output response of the system. For example, let us consider the microgrid with ten VCVSCs (shown in Fig. 13) and let us change the X/R ratio of line 3 while keeping its impedance modulus and the X/R ratio of all the other lines.

Fig. 16 shows the evolution of the state RC of the most relevant state of each line.

Fig. 16 shows that lines 1, 2 and 3 are much more relevant than lines 7, 8 and 9. The communication graph (from DG_i to DG_{i+1}, $i \in [1, 9]$) affects this result. In fact, if the graph is inverted (from DG_i to DG_{i-1}, $i \in [2, 10]$) the relevance of the lines is also inverted (see Fig. 17). Notice that the relevance of the line with an increasing X/R ratio always increases.

This information can help choose systematically which lines need detailed modelling and which ones can be simplified for each case study. This could be of interest for determining areas of influence for co-simulation, for instance.

6.2. Analysis of the selection of the input and output variables

Since the proposed method takes into consideration the input–output response of the system, results are affected by the outputs considered. Indeed, the selection of the input and output variables affects the RC since it affects the Gramians and consequently the transformation matrix **T**. In general, the selection of input and output variables may vary according to the study of interest. For example, to analyse the frequency stability of the system of Fig. 13, the frequency of the centre of inertia (COI) could be considered as an output.

Table 4 illustrates the influence of the output selection on the relevance of the 26 most relevant states of the system.

Table 4 shows that by adding COI's frequency to the initial output variable selection, the relevant states and their order hardly change. When choosing the frequency of the COI as the only output, frequency and active power dynamics are, however, the most relevant ones, whereas voltage dynamics are not that relevant. This makes sense since frequency dynamics are mainly affected by active power variations (and much less by voltage and reactive power variations).

To validate this result, the microgrid with 10 VCVSCs was reduced by considering COI's frequency as the only output and the frequency set point of the leader (DG1) as the input. The reduced model has 26 states which include all reference-frame angles but the leader's one (9), all secondary-control-related states (10) and those related to

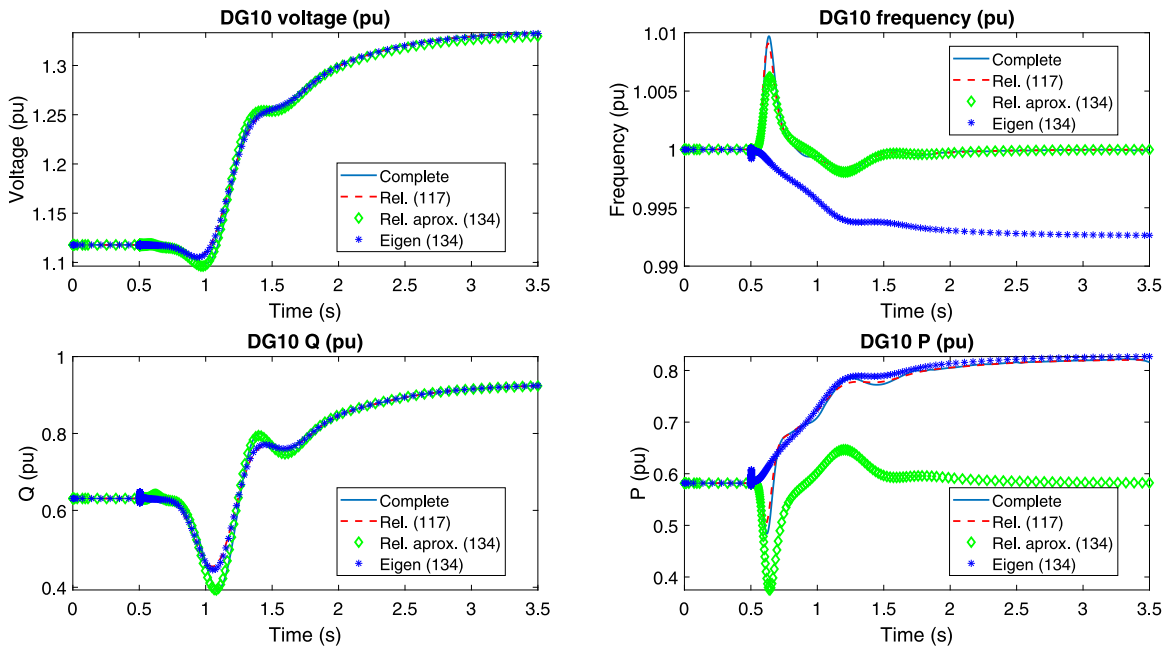

Fig. 15. Response of electrical variables of DG10 in the microgrid with ten VCVSCs (case study 2) to a 50% reduction of Load 1 impedance while maintaining its X/R ratio. The numbers enclosed within brackets in the legends show the number of states included in each reduced nonlinear model.

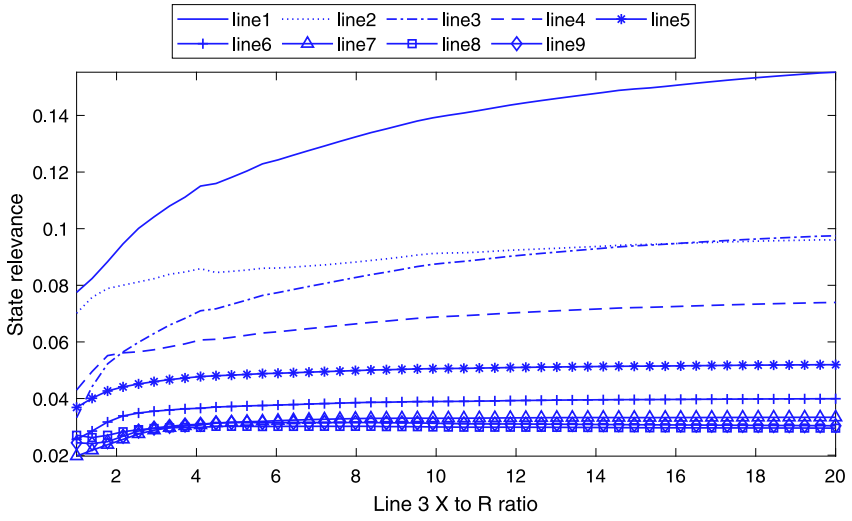

Fig. 16. Evolution of the state RC of the most relevant state of each line when changing the X/R ratio of line 3 while keeping its impedance modulus constant.

active-power filters for all DGs except DG7, DG8 and DG9 (7). The disturbance simulated consists of a 5% increment in the frequency set point of the leader (DG1) and Fig. 18 shows the response of the frequency of the COI for the original and the reduced nonlinear models to this disturbance. Fig. 18 also indicates, for each of the considered approaches, the number of states. "Rel." has the fewest states. Fig. 19 shows the Bode diagram for the linear approximations to the complete and reduced ("Rel.") nonlinear models with the input–output selection considered.

Since the other approaches do not focus on the input–output response of the system but only on the state matrix of a linear approximation of the original nonlinear system, they find the same relevant states as when considering the electrical variables of all VCVSCs as outputs and fail to follow the frequency dynamics with a reduced number of states.

7. Conclusions

This paper has proposed an algorithm to quantify the state relevance of a dynamic system while preserving the physical meaning of the state variables and has described possible applications to a microgrid with electronic power sources. The algorithm uses a balanced realisation of a linear approximation of the system to calculate the energy of each state variable in the output response. The transformation leading from the original linear system to the balanced realisation is linear, and system eigenvalues are invariant. Unfortunately, the states of the balanced realisation may not have physical meaning. The relevance of the original states is calculated through the participation factors of the system eigenvalues in the two sets of state variables, namely, before and after the transformation leading to the balanced realisation. The proposed algorithm has been applied to identify the relevant states

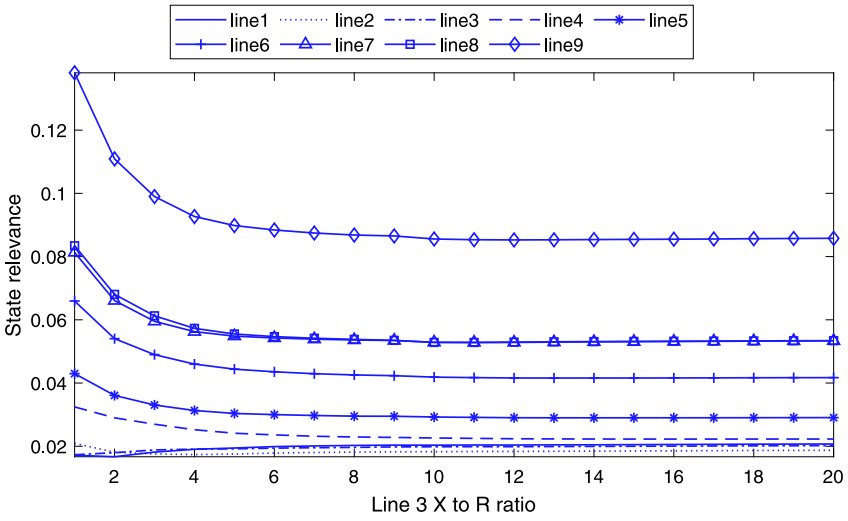

Fig. 17. Evolution of the state RC of the most relevant state of each line when changing the X/R ratio of line 3 while keeping its impedance modulus constant. Graph from DG10 (leader) to DG1.

Table 2
Case study 1 (2 VCVSCs). R_{x_1} and R_{x_2} are the state relevance calculated by "Rel" and "Rel. ap." approaches, respectively. x_3 gives the state order obtained by "Eig" approach. No clear time-scale separation.

State name	$R_{x,1}$	$R_{x,2}$	x_3
$DG2/\theta$	**1**	0.20265	9
$DG2/E^*$	**0.80611**	**0.84812**	**6**
$DG2/\omega^*$	**0.7537**	0.14393	10
$DG1/P_f$	**0.66905**	0.11802	18
$DG2/PIv_d$	**0.59128**	**0.76333**	**5**
$DG2/PIi_d$	**0.5815**	**0.75303**	**7**
$DG1/\omega^*$	**0.51843**	0.085096	19
$DG1/E^*$	**0.46321**	0.29667	11
$DG1/PIi_d$	0.21128	**0.38871**	12
$DG1/PIv_d$	0.20369	0.3861	**8**
$DG1/Q_f$	0.1972	0.1216	17
$DG1/i_{oq}$	0.18067	0.049342	13
$line/i_d$	0.1742	0.049568	43
$DG1/i_{od}$	0.17374	0.049969	44
$line/i_q$	0.17058	0.047488	14
$DG1/i_{ld}$	0.11985	0.031824	27
$DG1/i_{lq}$	0.10294	0.027054	28
$DG1/v_{od}$	0.074896	0.022417	26
$Delay-mpP(3)$	0.061444	0.013688	37
$DG1/v_{oq}$	0.045319	0.026989	29
$Delay-\omega(3)$	0.044722	0.0091235	36
$DG2/v_{od}$	0.027841	0.027275	24
$Load1/i_q$	0.025238	0.017029	20
$Load1/i_d$	0.023709	0.016606	21
$DG2/Q_f$	0.020457	0.066592	16
$DG2/P_f$	0.019911	0.051659	15
$Load2/i_q$	0.012315	0.016433	22
$Load2/i_d$	0.011226	0.015891	23
$Delay-nqQ(3)$	0.0106	0.008306	39
$DG2/i_{oq}$	0.010234	0.00342	42
$DG2/i_{od}$	0.0062695	0.0031477	41
$DG2/i_{lq}$	0.0036369	0.0053899	30
$DG1/PIi_q$	0.0027129	**0.98425**	**2**
$DG1/PIv_q$	0.0025971	**1**	**1**
$DG2/i_{ld}$	0.0024959	0.0053131	31
$Delay-\omega(2)$	0.0013242	0.0026039	32
$Delay-mpP(2)$	0.001292	0.0025898	33
$DG2/v_{oq}$	0.0012146	0.020922	25
$Delay-\omega(1)$	0.00076035	0.001508	35
$Delay-mpP(1)$	0.00074536	0.0014999	34
$DG2/PIv_q$	0.00025056	**0.99918**	**3**
$DG2/PIi_q$	0.00022255	**0.9834**	**4**
$Delay-nqQ(2)$	3.9989e−05	5.1843e−05	38
$Delay-nqQ(1)$	1.9983e−05	2.9065e−05	40

Table 3
Case study 1 (2 VCVSCs). R_{x_1} and R_{x_2} are the state relevance calculated by "Rel" and "Rel. ap." approaches, respectively. x_3 gives the state order obtained by "Eig" approach. Clear time-scale separation.

State name	$R_{x,1}$	$R_{x,2}$	x_3
$DG1/\omega^*$	**1**	**0.96606**	**1**
$DG2/\omega^*$	**0.91326**	**0.91722**	**2**
$DG2/E^*$	**0.69113**	**1**	**3**
$DG1/P_f$	**0.50268**	**0.59417**	**5**
$DG2/\theta$	**0.48854**	**0.57902**	**6**
$DG1/E^*$	**0.39584**	**0.52737**	**4**
$DG2/Q_f$	**0.24991**	**0.65226**	**7**
$DG2/P_f$	**0.23146**	**0.455**	**8**
$DG1/Q_f$	**0.1837**	**0.26013**	**9**
$DG1/PIv_d$	0.043904	0.099938	10
$DG1/PIi_d$	0.043367	0.098454	11
$DG2/PIi_d$	0.0088186	0.089091	13
$DG2/PIv_d$	0.0087562	0.09028	12
$DG1/i_{ld}$	0.0087091	0.004619	29
$Load1/i_d$	0.0078151	0.0023619	21
$Load1/i_q$	0.0077397	0.002271	20
$DG1/i_{od}$	0.0073217	0.0073633	43
$DG1/i_{lq}$	0.0073141	0.003001	28
$line/i_q$	0.0066516	0.0065061	19
$line/i_d$	0.0064484	0.0062382	18
$DG1/v_{od}$	0.0061259	0.0030799	26
$DG1/i_{oq}$	0.0057181	0.0055408	44
$DG1/v_{oq}$	0.0051427	0.0023077	27
$DG2/i_{oq}$	0.0017761	0.0022288	33
$Load2/i_q$	0.0013125	0.0027668	22
$Load2/i_d$	0.0010476	0.0025129	23
$DG1/PIi_q$	0.00058978	0.085032	17
$DG1/PIv_q$	0.00056472	0.086395	16
$DG2/i_{od}$	0.00033632	0.00053219	32
$DG2/v_{od}$	0.00019634	0.0019809	24
$DG2/PIv_q$	4.3818e−05	0.086013	14
$DG2/PIi_q$	4.3158e−05	0.084655	15
$Delay-mpP(3)$	1.5463e−05	1.6877e−05	40
$Delay-\omega(3)$	1.4707e−05	1.6103e−05	41
$DG2/i_{ld}$	4.5115e−06	0.0004148	31
$Delay-nqQ(3)$	3.2894e−06	5.0874e−06	42
$DG2/v_{oq}$	7.4e−07	0.0017938	25
$DG2/i_{lq}$	7.0284e−07	0.00042746	30
$Delay-mpP(1)$	3.3645e−08	9.8701e−07	39
$Delay-nqQ(1)$	2.4814e−08	7.5812e−07	37
$Delay-\omega(1)$	4.6621e−09	9.1807e−07	35
$Delay-mpP(2)$	1.0086e−11	1.6358e−06	38
$Delay-\omega(2)$	3.607e−12	1.5729e−06	34
$Delay-nqQ(2)$	1.4872e−12	1.2682e−06	36

Table 4
State relevance analysis for different output choices. Case 1 with v, θ, P and Q of both DGs as outputs. Case 2 adding COI as an output. Case 3 COI as the only output.

Case 1		Case 2		Case 3	
State name	R_x	State name	R_x	State name	R_x
$DG10/\theta$	1	$DG10/\theta$	1	$DG10/\theta$	1
$DG8/E^*$	0.99917	$DG8/E^*$	0.99245	$DG9/\theta$	0.66304
$DG7/E^*$	0.96861	$DG7/E^*$	0.96231	$DG4/\theta$	0.46822
$DG9/E^*$	0.96195	$DG9/E^*$	0.95529	$DG3/\theta$	0.44201
$DG6/E^*$	0.91497	$DG6/E^*$	0.90912	$DG8/\theta$	0.43829
$DG5/E^*$	0.87145	$DG5/E^*$	0.86564	$DG5/\theta$	0.43394
$DG10/E^*$	0.84936	$DG10/E^*$	0.84405	$DG3/\omega^*$	0.41449
$DG4/E^*$	0.81012	$DG4/E^*$	0.80456	$DG2/\omega^*$	0.40099
$DG3/E^*$	0.65407	$DG3/E^*$	0.65006	$DG4/\omega^*$	0.3672
$DG9/\theta$	0.64352	$DG9/\theta$	0.64418	$DG1/\omega^*$	0.34421
$DG3/\theta$	0.52128	$DG3/\theta$	0.5206	$DG8/\omega^*$	0.32143
$DG2/E^*$	0.51542	$DG4/\theta$	0.51357	$DG6/\theta$	0.31627
$DG4/\theta$	0.51349	$DG2/E^*$	0.51314	$DG7/\theta$	0.31583
$DG5/\theta$	0.51163	$DG5/\theta$	0.51116	$DG9/\omega^*$	0.3046
$DG2/\omega^*$	0.5023	$DG2/\omega^*$	0.50207	$DG2/\theta$	0.29939
$DG8/\theta$	0.48347	$DG8/\theta$	0.48343	$DG1/P_f$	0.2903
$DG10/PIv_d$	0.47034	$DG3/\omega^*$	0.46884	$DG5/\omega^*$	0.28934
$DG3/\omega^*$	0.46835	$DG10/PIv_d$	0.46762	$DG7/\omega^*$	0.28185
$DG10/PIi_d$	0.46319	$DG10/PIi_d$	0.46051	$DG10/P_f$	0.21092
$DG9/PIv_d$	0.45552	$DG9/PIv_d$	0.45257	$DG10/\omega^*$	0.19797
$DG9/PIi_d$	0.4488	$DG9/PIi_d$	0.44589	$DG6/\omega^*$	0.19175
$DG4/PIv_d$	0.43982	$DG4/PIv_d$	0.43689	$DG4/P_f$	0.16695
$DG4/PIi_d$	0.43279	$DG4/PIi_d$	0.42991	$DG5/P_f$	0.1617
$DG3/PIv_d$	0.42718	$DG3/PIv_d$	0.42456	$DG2/P_f$	0.15137
$DG3/PIi_d$	0.42015	$DG6/\theta$	0.41911	$DG6/P_f$	0.14556
$DG6/\theta$	0.42015	$DG7/\theta$	0.41894	$DG3/P_f$	0.14243

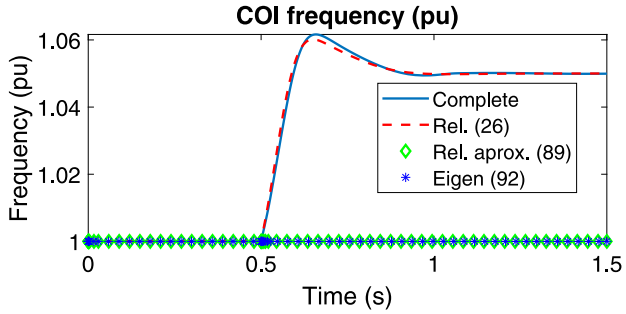

Fig. 18. Response of the frequency of the COI in case study 2 (10 VCVSCs) to a 5% increment in the frequency set point of DG1 (leader). The numbers enclosed within brackets in the legends show the number of states included in the reduced nonlinear models.

in two case studies, and the full nonlinear models have been reduced by relying on this information and by assuming that the derivative of less-relevant states can be made equal to zero and controlled variables follow their references. Results show that the traditional approach of associating relevant states with slow dynamics while fast dynamics are ignored requires reduced-order models of a higher order than those obtained with the proposed state-selection approach if similar simulation accuracy of small disturbances is sought. The two approaches to state selection produce the same results if there is a clear time-scale separation of the system dynamics; therefore, the proposed state-relevance coefficient can be used to systematically choose the states to include in a reduced model while it provides valuable information for the modal analysis of the system. Needless to say, the state relevance depends on the choice of inputs and outputs (*i.e.*, it is application-dependent).

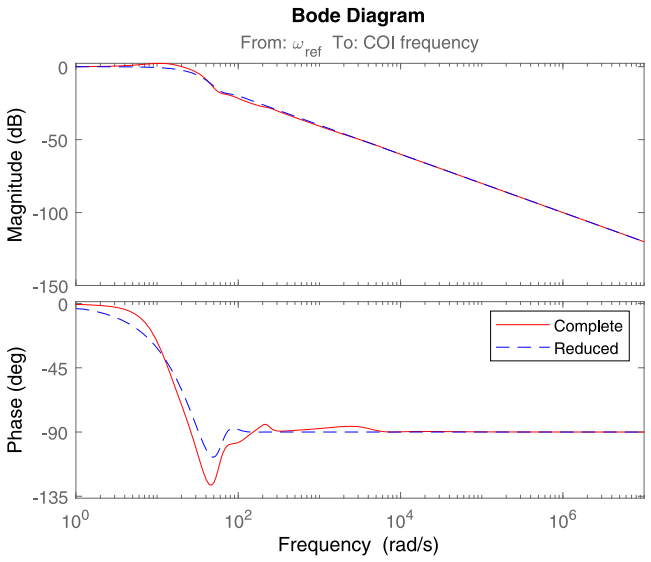

Fig. 19. Bode diagram of the system using the increment in the frequency set point of DG1 (leader) as input and the frequency of the COI as output.

Table A.5
Operating point of the microgrid of case 1. $i \in [1–2]$.

State name	Value	State name	Value
DGi/P	0.50457 pu	DGi/Q	0.53963 pu
$DG1/v$	1 pu	$DG1/\theta$	0 rad
$DG2/v$	1.0452 pu	$DG2/\theta$	0.034023 rad

CRediT authorship contribution statement

Andrés Tomás-Martín: Conceptualization, Methodology, Software, Data curation, Writing – original draft. **Aurelio García-Cerrada:** Supervision, Funding acquisition, Methodology, Validation, Writing – review & editing. **Lukas Sigrist:** Supervision, Funding acquisition, Methodology, Validation, Writing – review & editing. **Sauro Yagüe:** Methodology, Visualization, Data curation. **Jorge Suárez-Porras:** Methodology, Data curation, Writing – review & editing.

Declaration of competing interest

The authors declare that they have no known competing financial interests or personal relationships that could have appeared to influence the work reported in this paper.

Data availability

Data will be made available on request.

Appendix A. Operating points used for the linearisation of the microgrids of case studies 1 and 2

Tables A.5 and A.6 show the operating points used for the linearisation in both case studies, given as power-flow solutions.

Appendix B. Complete nonlinear model of a VCVSC

Fig. B.20 includes the complete nonlinear model of a VCVSC in a d-q reference frame. Each VCVSC and its control are modelled in a reference frame synchronously rotating with its filter capacitor voltage $v_{o(dq)i}$, and $v_{oqi} = 0$ in steady state; however, the grid-side inductance of the LCL filter is modelled in the absolute reference frame, which rotates synchronously with DG1's output-capacitor voltage (*i.e.*, for DG1, $\theta_i =$

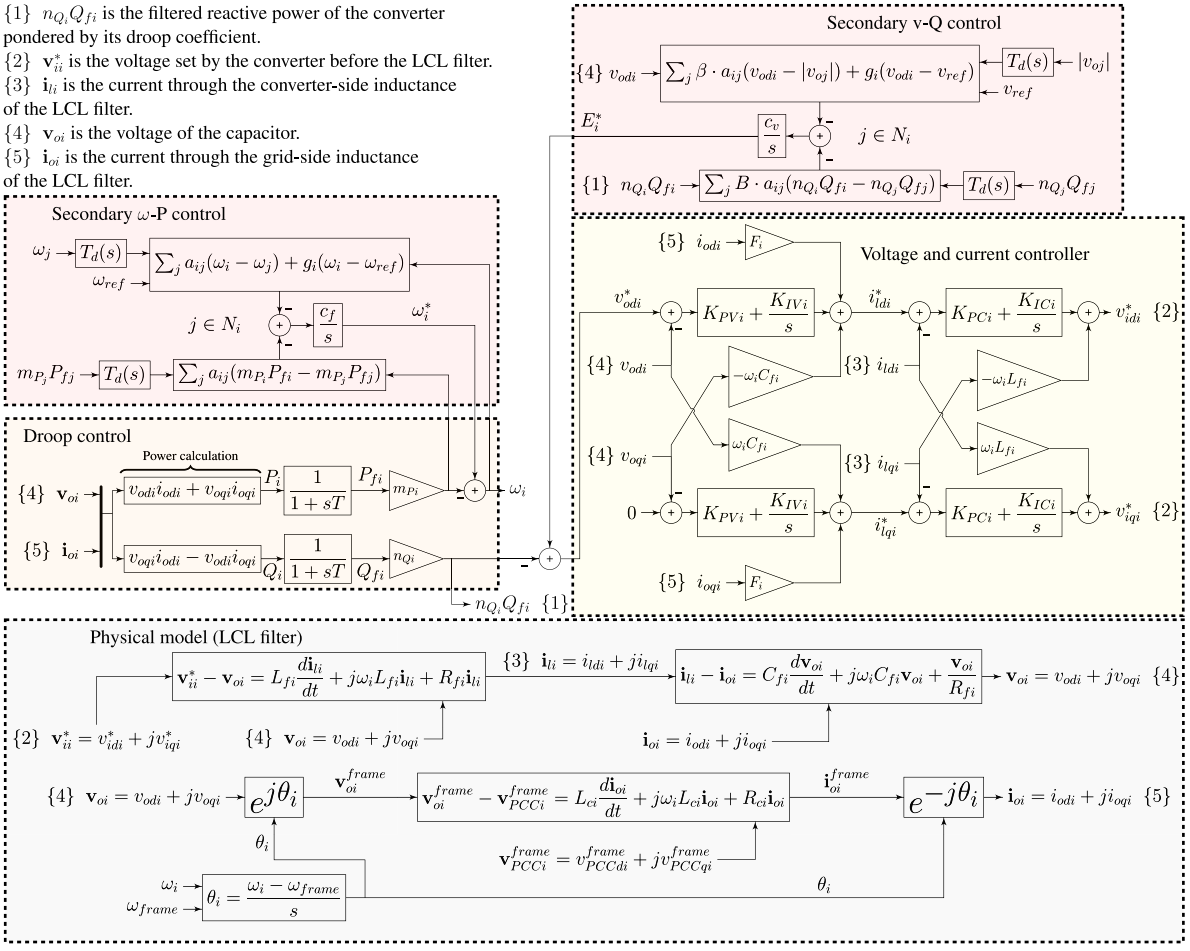

Fig. B.20. Complete nonlinear model of a VCVSC with LCL filter in a d-q reference frame.

Table A.6
Operating point of the microgrid of case 2. $i \in [1\text{–}10]$.

State name	Value	State name	Value
DGi/P	0.58174 pu	DGi/Q	0.63089 pu
$DG1/v$	1 pu	$DG1/\theta$	0 rad
$DG2/v$	1.0349 pu	$DG2/\theta$	0.026235 rad
$DG3/v$	1.0606 pu	$DG3/\theta$	0.042931 rad
$DG4/v$	1.0792 pu	$DG4/\theta$	0.053505 rad
$DG5/v$	1.0927 pu	$DG5/\theta$	0.060102 rad
$DG6/v$	1.1024 pu	$DG6/\theta$	0.064119 rad
$DG7/v$	1.1091 pu	$DG7/\theta$	0.06648 rad
$DG8/v$	1.1137 pu	$DG8/\theta$	0.067801 rad
$DG9/v$	1.1165 pu	$DG9/\theta$	0.068483 rad
$DG10/v$	1.1178 pu	$DG10/\theta$	0.068768 rad

0). Variables referred to the absolute reference frame can be referred to any DGi's reference frame by multiplying by $e^{-j\theta_i}$ and the latter can be referred to the former by multiplying by $e^{j\theta_i}$.

Appendix C. Reducing the number of states in the nonlinear model

Electrical elements with no dynamics

The differential equations of a balanced inductor with an inductance value L and a series resistance R in a $d-q$ reference frame which rotates with a variable angular speed $\omega(t)$ are [3]:

$$\begin{cases} v_d(t) = L\dfrac{di_d(t)}{dt} - \omega(t)Li_q(t) + Ri_d(t) \\ v_q(t) = L\dfrac{di_q(t)}{dt} + \omega(t)Li_d(t) + Ri_q(t) \end{cases} \tag{C.1}$$

Notice that d and q components of electrical variables can be gathered together in a complex number to have a compact expression:

$$\mathbf{v}(t) = L\frac{d\mathbf{i}(t)}{dt} + j\omega(t)L\mathbf{i}(t) + R\mathbf{i}(t) \tag{C.2}$$

where $\mathbf{v}(t) = v_d(t) + jv_q(t)$ is the instantaneous voltage difference between the inductor terminals, and $\mathbf{i}(t) = i_d(t) + ji_q(t)$ is the instantaneous current through the inductor. The term $j\omega(t)L\mathbf{i}$ calculates the cross-coupling between the d and q components of the inductor differential equations.

If the inductor dynamics are very fast, currents quickly reach their steady-state value (where $d\mathbf{i}(t)/dt = 0$) and can be calculated from the applied voltage as the following complex number:

$$\mathbf{i}(t) = \frac{\mathbf{v}(t)}{j\omega(t)L + R} \tag{C.3}$$

where $j\omega(t)L + R$ is not a typical frequency-dependent impedance but the operator that relates instantaneous $d-q$ voltage components with instantaneous $d-q$ current components in a reference frame that rotates with an angular speed equal to $\omega(t)$.

Similarly, $d-$ and q-axis differential equations for a balanced capacitor of capacitance C and a parallel resistance R can be obtained, respectively, from the real and imaginary parts of :

$$\mathbf{i}(t) = C\frac{d\mathbf{v}(t)}{dt} + j\omega(t)C\mathbf{v}(t) + \frac{\mathbf{v}(t)}{R} \tag{C.4}$$

where $\mathbf{v}(t) = v_d(t)+jv_q(t)$ is the voltage difference between the capacitor terminals, and $\mathbf{i}(t) = i_d(t) + ji_q(t)$ is the total current through the capacitor.

If the capacitor dynamics are very fast, the voltage will quickly reach its steady state value (where $d\mathbf{v}(t)/dt = 0$), yielding:

$$\mathbf{v}(t) = \frac{\mathbf{i}(t)}{j\omega(t)C + 1/R} \tag{C.5}$$

where $j\omega(t)C + 1/R$ is not a typical frequency-dependent admittance, either, but allows the calculation of the $d-$ and q-axis instantaneous voltage components immediately after the instantaneous current components through the capacitor are known.

Notice that d and q components of all balanced electrical variables will have a constant value in steady state if and only if $\omega(t)$ is eventually equal to the power system frequency.

Voltage and current controllers

If current-controller dynamics are not relevant, but the voltage-controller dynamics are relevant, the model of a VSC can be simplified by assuming that the converter output currents follow their set points (*) instantaneously:

$$i^*_{ldi} = i_{ldi} \;\; \& \;\; i^*_{lqi} = i_{lqi} \tag{C.6}$$

Similarly, if the dynamics of the voltage controllers are not relevant, the model of a VSC can be simplified further as:

$$v^*_{odi} = v_{odi} \;\; \& \;\; v^*_{oqi} = v_{oqi} \tag{C.7}$$

where the output voltages ($d-q$ components) reach their set points (*) immediately.

Primary and secondary control

If the dynamics of the low pass filters of the active- and reactive-power measurements are not found to be relevant, those filters can be omitted. If the frequency (or voltage) secondary controller of a VSC is not found to be relevant, the frequency (voltage) set point of the converter remains constant.

References

[1] Kundur P, Balu NJ, Lauby MG. Power System Stability and Control. The EPRI power system engineering series, New York: McGraw-Hill; 1994.

[2] Ghosh S, Senroy N. A comparative study of two model order reduction approaches for application in power systems. In: 2012 IEEE power and energy society general meeting. 2012, p. 1–8. http://dx.doi.org/10.1109/PESGM.2012.6344785.

[3] Qoria T, Cossart Q, Li C, Guillaud X, Colas F, Gruson F, et al. WP3 - control and operation of a grid with 100% converter-based devices. Deliverable 3.2: Local control and simulation tools for large transmission systems. Tech. rep., MIGRATE project; 2018, p. 40–52, URL https://www.h2020-migrate.eu/downloads.html. [Accessed 05 May 2022].

[4] Karawita C, Annakkage UD. A hybrid network model for small signal stability analysis of power systems. IEEE Trans Power Syst 2010;25(1):443–51. http://dx.doi.org/10.1109/TPWRS.2009.2036709.

[5] Grdenić G, Delimar M, Beerten J. Assessment of AC network modeling impact on small-signal stability of AC systems with VSC HVDC converters. Int J Electr Power Energy Syst 2020;119:105897. http://dx.doi.org/10.1016/j.ijepes.2020.105897.

[6] Grdenić G, Delimar M, Beerten J. AC Grid model order reduction based on interaction modes identification in converter-based power systems. IEEE Trans Power Syst 2022. http://dx.doi.org/10.1109/TPWRS.2022.3180426.

[7] Wang X, Blaabjerg F. Harmonic stability in power electronic-based power systems: Concept, modeling, and analysis. IEEE Trans Smart Grid 2019;10(3):2858–70. http://dx.doi.org/10.1109/TSG.2018.2812712.

[8] Bayo Salas A. Control interactions in power systems with multiple VSC HVDC converters. Analysis, modelling and mitigation of electromagnetic stability problems [Ph.D. thesis], KU Leuven: Arenberg Doctoral School, Faculty of Engineering Science; 2018.

[9] Beerten J, D'Arco S, Suul JA. Frequency-dependent cable modelling for small-signal stability analysis of VSC-HVDC systems. IET Gener Transm Distrib 2016;10(6):1370–81. http://dx.doi.org/10.1049/iet-gtd.2015.0868.

[10] Laub A, Heath M, Paige C, Ward R. Computation of system balancing transformations and other applications of simultaneous diagonalization algorithms. IEEE Trans Automat Control 1987;32(2):115–22. http://dx.doi.org/10.1109/TAC.1987.1104549.

[11] Ramirez A, Mehrizi-Sani A, Hussein D, Matar M, Abdel-Rahman M, Jesus Chavez J, et al. Application of balanced realizations for model-order reduction of dynamic power system equivalents. IEEE Trans Power Deliv 2016;31(5):2304–12. http://dx.doi.org/10.1109/TPWRD.2015.2496498.

[12] Antoulas AC. Approximation of large-scale dynamical systems. Philadelphia: Society for Industrial and Applied Mathematics; 2005.

[13] Olfati-Saber R, Murray R. Consensus problems in networks of agents with switching topology and time-delays. IEEE Trans Automat Control 2004;49(9):1520–33. http://dx.doi.org/10.1109/TAC.2004.834113.

[14] Kokotović P, Khalil HK, O'Reilly J. Singular perturbation methods in control: Analysis and design. Society for Industrial and Applied Mathematics; 1999, http://dx.doi.org/10.1137/1.9781611971118.

[15] Rasheduzzaman M, Mueller JA, Kimball JW. Reduced-order small-signal model of microgrid systems. IEEE Trans Sustain Energy 2015;6(4):1292–305. http://dx.doi.org/10.1109/TSTE.2015.2433177.

[16] Durić M, Radojević Z, Turković E. A practical approach to the order reduction of a power system model for small signal stability analysis. Electr Power Syst Res 1997;41(1):13–8. http://dx.doi.org/10.1016/S0378-7796(96)01137-6.

[17] Parang B, Mohammadi M, Arefi MM. Residualisation-based model order reduction in power networks with penetration of photovoltaic resources. IET Gener Transm Distrib 2019;13(13):2619–26. http://dx.doi.org/10.1049/iet-gtd.2018.6172.

[18] Jayawardena AV, Meegahapola LG, Robinson DA, Perera S. Representation of a grid-tied microgrid as a reduced order entity for distribution system dynamics and stability studies. Int J Electr Power Energy Syst 2015;73:591–600. http://dx.doi.org/10.1016/j.ijepes.2015.05.040.

[19] Moore B. Principal component analysis in linear systems: Controllability, observability, and model reduction. IEEE Trans Automat Control 1981;AC-26(1):17–32. http://dx.doi.org/10.1109/TAC.1981.1102568.

[20] Sauer PW, Pai MA. Power system dynamics and stability. Upper Saddle River, N.J: Prentice Hall; 1998, Chap. 8.

[21] Pérez-Arriaga I, Verghese G, Schweppe F. Selective modal analysis with applications to electric power systems, PART I: Heuristic introduction. IEEE Trans Power Appar Syst 1982;PAS-101(9):3117–25. http://dx.doi.org/10.1109/TPAS.1982.317524.

[22] Gusrialdi A, Qu Z. Distributed estimation of all the eigenvalues and eigenvectors of matrices associated with strongly connected digraphs. IEEE Control Syst Lett 2017;1(2):328–33. http://dx.doi.org/10.1109/LCSYS.2017.2717799.

[23] Bidram A, Davoudi A, Lewis FL. A Multiobjective distributed control framework for islanded AC microgrids. IEEE Trans Ind Inf 2014;10(3):1785–98. http://dx.doi.org/10.1109/TII.2014.2326917.

[24] Bidram A, Davoudi A, Lewis FL, Guerrero JM. Distributed cooperative secondary control of microgrids using feedback linearization. IEEE Trans Power Syst 2013;28(3):3462–70. http://dx.doi.org/10.1109/TPWRS.2013.2247071.

[25] Bidram A, Nasirian V, Davoudi A, Lewis FL. Cooperative synchronization in distributed microgrid control. Advances in industrial control, Cham, Switzerland: Springer International Publishing; 2017, http://dx.doi.org/10.1007/978-3-319-50808-5, Chap. 3.

[26] Simpson-Porco JW, Shafiee Q, Dorfler F, Vasquez JC, Guerrero JM, Bullo F. Secondary frequency and voltage control of islanded microgrids via distributed averaging. IEEE Trans Ind Electron 2015;62(11):7025–38. http://dx.doi.org/10.1109/TIE.2015.2436879.

[27] Hossain MA, Pota HR, Hossain MJ, Blaabjerg F. Evolution of microgrids with converter-interfaced generations: Challenges and opportunities. Int J Electr Power Energy Syst 2019;109:160–86. http://dx.doi.org/10.1016/j.ijepes.2019.01.038.